Egypt. J. Chem. **Vol. 67**, No. 1 pp. 205 - 223 (2024)

Egyptian Journal of Chemistry

http://ejchem.journals.ekb.eg/

Cationic Organoclay for Efficient Concomitant Removal of Anionic Dyes in Batch and Column modes: Adsorption Characteristics and Mechanism Study

Magda A. Akl[1*], Nora A. El Mahdy[1], Mohammed Al-Awadhi[2] and Aya G. Mostafa[1]

[1]*Department of Chemistry, Faculty of Science, Mansoura University, Mansoura 35516, Egypt*

[2]*Department of Chemistry, Faculty of Education & Science, Saba Region University, Marib, Yemen*

Abstract

This study aimed to create an organoclay [MMT@CTAB] by mixing the naturally occurring mineral montmorillonite [MMT] with the cationic surfactant cetyltrimethylammonium bromide [CTAB]. FTIR spectroscopy, elemental analysis and scanning electron microscopy [SEM] have been employed to analyze both the unmodified MMT and the MMT that has been modified using CTAB [MMT@CTAB]. The MMT@CTAB adsorbent was investigated for the removal of methyl orange (MO) and Rose Bengal (RB) anionic dyes (in single and/or in multi-components solutions) and additionally, in batch and column modes. Certain variables that impact the adsorption process, such as initial dye concentration, contact time, temperature, pH, and adsorbent dose, are evaluated. The kinetic investigation, which is characterized by a pseudo-second-order kinetic model, reveals that equilibrium adsorption of MO and RB dyes onto MMT@CTAB may be attained in 60 and 120 minutes, respectively. MO and RB were expected to achieve maximum adsorption efficiencies of 98.7 and 98.4%, respectively, at 100 and 150 mgL^{-1} concentrations, a dosage of 0.5 gL^{-1} adsorbent, and an initial pH of 7. In addition, Langmuir model best fits the sorption isotherm data, with the maximum adsorption capacity at 303 K being 203.25 mg g^{-1} for MO and 304.878 mg g^{-1} for RB, as shown by the non-linear form of Langmuir isotherm. Regenerated MMT@CTAB may be used for at least four more adsorption/desorption cycles, with ethanol indicating to be the most effective regeneration eluent. Each anionic dye was subjected to a binary systematic analysis. Since the adsorption of these anionic dyes onto MMT@CTAB was reduced when the temperature was increased, thermodynamic evidence suggests that adsorption is an exothermic, spontaneous process. The prepared cationic organoclay MMT@CTAB was successfully applied for the removal of MO and RB from real water samples and synthetic effluents with a recovery % more than 95%. The plausible adsorption mechanism of MO and RB onto MMT@CTAB is proposed to be due to electrostatic interaction and hydrogen bond formation. Finally, our study shows that MMT@CTAB may be employed efficiently and effectively to remove anionic dyes from a wide range of the collected real water samples.

Keywords: montmorillonite, organoclay, CTAB, methyl orange (MO), Rose Bengal (RB), anionic dyes, adsorption, wastewater

1. Introduction

Globally, we not only need to deal with water deficiency, but also the problem of water pollution from hazardous toxins [1, 2]. Sewage discharge has increased as well due to fast industrial growth. Hazardous aromatic compounds, metals, and dyes are only some of the organic and inorganic components found in these wastewaters [3–6]. Some dyes and pigments have been labeled as hazardous compounds due to their potential toxicity to human health. They are harmful, consume a long time to decompose in landfills or water treatment plants, and impair water transparency [7,8]. As, there is enough evidence that prolonged exposure to dyes and their compounds may cause cancer and other serious health problems. Furthermore, the disruption of the photosynthetic cycle induced by textile effluent in water ways disrupts the delicate balance of aquatic life and the food chain [9].

Methyl orange [$C_{14}H_{14}N_3NaO_3S$, MO] is a kind of acidic anionic single- dye that has been persistently employed in a variety of commercial applications, including textiles, experimental studies, and other industries [10].This dye is toxic to marine life [11]. The symptoms of acute exposure to this toxic dye in humans include a rapid heart rate, nausea, vomiting, shock, cyanosis, jaundice, quadriplegia, and tissue necrosis [12, 13]. Rose Bengal [$C_{20}H_4Cl_4I_4O_5$, RB] is a dark pink powder with several applications in the textile, plastic, printing, cosmetic, and fluorescent industries [14]. It is hydrophilic, organic, anionic, water -soluble and odourless powder. It causes inflammation and swelling of eyes, as well as

*Corresponding author e-mail: magdaakl@yahoo.com

Receive Date: 11 May 2023, Revise Date: 08 June 2023, Accept Date: 19 June 2023

DOI: 10.21608/EJCHEM.2023.210347.7962

skin irritation, itching, and blistering in humans by attacking the epithelium that lines the cornea [15]. The cytotoxic effects of Rose Bengal may be shown in many different cell systems [16]. Companies involved in the use and synthesis of MO & RB must thus take great care to eliminate toxic dyes from their wastewaters before dumping them into the environment. Methodologies [17] including photocatalytic degradation [18, 19], electrochemical oxidation [20], solvent extraction [21], membrane filtration [22], Fenton [23] and adsorption have proven efficient in cleaning up industrial wastewaters before they are released into the environment [24–27]. Adsorption has recently been shown to be favored over other methods owing to its simple operation, low cost, adaptability in design, and insensitivity to harmful pollutants [28]. Environmentally beneficial industrial processes may be eliminated, recovered, and recycled. The selection of adsorbents is crucial to the process's technical applicability and economic viability [3,13]. Wastewater decontamination may make use of non-traditional adsorbents, including natural materials, agricultural industry wastes, carbon materials, and bio sorbents. Activated carbon has been the most popular adsorbent due to its high capacity for absorbing organic dyestuffs [29]. Native and modified clay, notably montmorillonite, are being investigated as low-cost alternatives to activated carbon because of its high cost [30].

The smectite mineral montmorillonite is a phyllosilicate with two SiO_4^- tetrahedral sheets sandwiching an AlO_6^- octahedral sheet; it is extremely soft [type 2:1]. In the tetrahedral layer, Al^{3+} replaces Si_4^+, and in the octahedral layer, Mg^{2+} replaces Al^{3+}, giving the material a permanent negative charge [25]. The presence of exchangeable cations [that is, Na^+, Ca^{2+}] in crystal lattices counteracts this negative charge, ensuring the material's efficacy in the ion-exchange adsorption of cationic contaminants [31]. These exchangeable cations become highly hydrated in water, creating a hydrophilic atmosphere on the clay surface [32]. For cationic dyes, MMT clay has been shown to have a high sorption capacity [33].

Herbicide adsorption studies have focused mostly on negative-charged, expandable layered silicates like montmorillonite [MMT] since these clays are widely accessible, cheap, and easy to extract, non-toxic, and mechanically and chemically stable [34]. Native MMT is poor for eliminating anionic and hydrophobic contaminants from aqueous solutions, because of their negative charges and hydrophilic surface characteristics. Adsorption capacity of native MMT for removal of anion pollutants from water [e.g., anionic dyes] may be improved by modifying the surface of native MMT with organic components. To modify the surface properties of clay, such as its charge, hydrophobicity, and cation exchange capacity, a cationic surfactant such cetyltrimethylammonium bromide $[[C_{16}H_{33}]N[CH_3]_3]Br$, CTAB] is often utilized [35,36].The effectiveness of MMT@CTAB in eliminating anionic dyes has been shown in a variety number of research studies[19,25,34,37,38].

Consequently, the novelty of this work is in the experimental [batch and column] investigation of anionic RB dye adsorption utilizing MMT modified by CTAB in aqueous solutions. Furthermore, the binary system is employed for both anionic MO and RB dyes. Additionally, both batch and column adsorption experiments of MO and RB are compared with one another. This current work utilized FTIR, SEM, elemental analysis, and nitrogen [N_2] sorption to evaluate and contrast the properties of Native MMT and modified [MMT@CTAB]. Several factors were studied to see how much of an impact they had on removal performance: adsorbent dosage, pH, initial MO&RB concentrations, and ionic strength [Na_2CO_3, NaCl, and EDTA]. To understand the adsorption mechanism and highest adsorption ability for MMT@CTAB, adsorption isotherm and kinetic experiments were conducted.

2 .Experimental

2.1 .Materials

In this work, the used MMT was collected from Egypt and was crushed and sieved using a 200-mesh screen that permits the passage of particles with size < 74 microns. The used chemicals are NaOH, HCl, KCl, Na_2CO_3, ethanol, Rose Bengal anionic dye, Methyl orange, and cetyl trimethylammonium bromide [CTAB] surfactant with Mwt equaling 364.4 g/mol. All these chemicals were obtained from Sigma Aldrich and were analytical grade

.

2.2. Characterizations

Utilizing a Perkin Elmer 550 spectrophotometer for determining Anionic dyes [MO and RB] Concentration over a range of 200-900 nm using quartz cells. The λ_{max} of MO is 466, RB: 549 nm, and (RB+MO):547nm**. The FTI**R spectra of native MMT, MMT@CTAB, MMT@CTAB-MO and MMT@CTAB-RB were investigated by [Perkin-Bhaskar-Elmer Co., USA]. Clay samples were grounded and mixed with KBr then pressed in pellets form. [JSM-6510LV model] was utilized for the investigation of samples [native MMT and MMT@CTAB] surface morphology. Estimation of the CNH composition for the MMT, MMT@CTAB was obtained by a Costech [ECS-4010] elemental analyzer. **The** pH_{PZC} of MMT@CTAB was determined as follows: 0.1g of the MMT@CTAB

clay adsorbent was added to a 25 ml of pH-adjusted NaCl [0.01 M] solution that varied from 2 to 12 and the mixtures were allowed to shake at the equilibrated shaker for 48 hours. 0.1 M of HCl and 0.1 M of NaOH were utilized for NaCl pH adjustment. After the shaking, the final pH was recorded and ΔpH was measured as in the following Eq [$\Delta pH = pH_i - pH_f$] and was plotted against the initial pH [pH_i]. The pH_{PZC} value is the cross point where the curve ΔpH vs pH_i crosses the line ΔpH = 0 [38].

2.3. Preparation of MMT@CTAB adsorbent

Here, the MMT@CTAB adsorbent was prepaed according to the approach given by [38, 39]. The first step in organo-montmorillonite [MMT@CTAB] synthesis was the dispersion of 25 g of the native MMT clay in dist.H_2O for 60 min. Then the next step was to gradually add to the suspended MMT an amount corresponding to 1 mmol/g CEC [cation exchange capacity]. The MMT and CTAB mixture was allowed to stir at 60°C for 6 hours. Then the mixture was centrifuged with speed 3000 rpm and washed many times by the dist.H_2O in order to remove any excess of the CTAB surfactant. The last step was to dry the produced MMT@CTAB powder for 24 hours in an oven at 70°C.

2.4. Adsorption procedures

2.4.1. Batch tests

The λ_{max} of methyl orange [MO], Rose Bengal [RB], and MO-RB anionic dyes mix were obtained through the scanning of their solutions in the range of [190-1100nm]. MO [466 nm], RB [549 nm] dye adsorption studies were performed with two different anionic dyes at concentrations ranging from 25 to 400 mg/L. For dye mixture adsorption experiment, the two dyes were mixed: 150 mg/L RB and 100 mg/L MO. The adsorption of MO and RB experiments were occurred in 125 ml stoppered bottles that contained 10 ml of anionic dye solution and adsorbent MMT@CTAB dose [0.005g]. Then, these bottles were shaken at 150 rpm on a thermostat shaker at room temperature. After the equilibrium was reached, the solutions were centrifuged at 3000rpm. The supernatant solution that includes the remains of both anionic dyes were measured at the λ_{max} for MO [466 nm] and RB [549 nm]. Samples after adsorption were scanned regularly between 200 and 900 nm at different time intervals to obtain the lambda maximum. Various parameters were studied such as contact time [15-240 min], temperature [25-45 °C], MMT@CTAB adsorbent dose [0.0025-0.05 g], pH [from 2 to 11 for MO and from 3 to 11 for RB], ionic strength, and initial concentration of dye [25-400 mg/l]. The anionic dye removal percentage [R, [%]] and adsorption capacity [q_e] of dyes were calculated as per Eq. [1] and Eq. [2], respectively [19].

$$R\,(\%) = \frac{C_i - C_f}{C_i} \times 100 \qquad [1]$$

$$q_e = \frac{(C_i - C_f) \times v}{wt} \qquad [2]$$

where C_i [mg/L] and C_f [mg/L] are the initial anionic dyes concentration and equilibrium anionic dyes concentration, respectively. V [L], is the volume of investigated dye and wt [g], is the MMT@CTAB dose.

2.4.2. Desorption and regeneration investigation

After the MO and RB dyes adsorption by MMT@CTAB clay, the investigated dyes desorption was examined by different eluents including ethanol, NaOH [0.2 mol/L], and sod. bicarbonate [0.2 mol/L], and HCl [0.2 mol/L]. The MMT@CTAB regeneration was examined through five repeated cycles of adsorption-desorption by the batch method. 0.005 g of MMT@CTAB was shaken with 10 ml of [100mg/L for MO and 150mg/L for RB] for 60 min for MO and 120 min for RB; then adsorbent was filtered and then it was eluted with absolute ethanol and these procedures were repeated for another 4 cycles. The anionic dyes [MO and RB] desorption [D[%]] MMT@CTAB was calculated from Eq. [3] [27].

$$\text{De-sorption } \% = \frac{amount\ dseorbed\ to\ the\ solution\ [mg/l]}{amount\ adsorbed\ on\ MMT@CTAB\ [mg/l]} \times 100 \qquad [3]$$

2.4.3. Column investigations

The use of MMT@CTAB clay as a filter was investigated through the column experiments studying. MMT@CTAB was pressed and put in the column bottom. The investigation of the optimum parameters as column diameter [0.7 and 0.9 cm], clay weight which varied from 0.002g to 0.02g, and the anionic dyes flow rate [slow and fast flow rates] have occurred at the anionic species [MO [100 mg/L] and RB [150 mg/L]] optimum pH that was obtained from the batch investigations. MO and RB concentration after passage through the column was determined at the spectrophotometer instrument, each one at its specific λ_{max}. The removal percentage [R[%]] was determined as in Eq. 1, [19].

2.5. Kinetics, isothermal, and thermodynamics studying

2.5.1. Initial concentration and isothermal investigation

The isothermal investigations for MO and RB adsorption occurred by placing 0.005g of MMT@CTAB clay adsorbent in a series of bottles involving the MO and RB dye solution. The initial dye concentration was in the range of [25-400 mg/L]. The previous bottles were placed in a shaker [thermostated] with a shaking speed of 150 rpm at 25°C for 60 min for MO and 120 min for RB at pH 7.

Langmuir and Freundlich's isothermal models were applied in the linear form and were calculated as shown in Eq. [4] and Eq. [5], respectively. Langmuir separation factor [RL] which presents in Eq. [6], is an essential parameter. It used in adsorbent-sorbate affinity prediction. Values of RL indications are illustrated as follows: if it is greater than 1.0 this means the unsuitability of the investigated adsorbent, while if it occurred in the range from 0 to 1 it means the suitability of the utilized adsorbent[19].

$$\frac{C_e}{q_e} = \frac{1}{k_L q_m} + \frac{C_e}{q_m} \quad [4]$$

$$\ln q_e = lnK_f + \frac{1}{n} lnC_e \quad [5]$$

$$R_l = \frac{1}{1+K_l C_o} \quad [6]$$

As, C_e [mg/L] is the anionic dyes [MO and RB] concentration at equilibrium, q_e [mg/g] is the dye capacity at equilibrium, q_m [mg/g] adsorption maximum amount, 1/n is the heterogeneity factor, while K_L [L/g] and K_F [L/g] are Langmuir and Frendlich constants.

2.5.2. Contact time and kinetic

For estimation of the adsorption rate-limiting step, kinetic investigations were carried out using two kinetic models; are pseudo-1st-order and pseudo-2nd-order which are presented in [Eq. [7]] and [Eq. [8]], respectively[40].The investigations occurred at the optimum pH for each dye [MO and RB] using 10 ml [100mg/L of MO and 150 mg/L of RB] and 0.005 g of the MMT@CTAB adsorbent which were allowed to shake with different contact times varied from 15 min to 240 min in a thermostated shaker at the room temperature with constant speed 150 rpm.

$$\frac{1}{q_t} = \frac{K_1}{q_e t} + \frac{1}{q_e} \quad [7]$$

$$\frac{t}{q_t} = \frac{1}{K_2 q_e^2} + \frac{t}{q_e} \quad [8]$$

The adsorption efficiency for MO and RB at equilibrium and at a certain time t [min] is expressed as q_e [mg/g] and q_t [mg/g], respectively. Also, K_1 and K_2 are constants for pseudo-1st-order and pseudo-2nd-order, respectively.

2.5.3. Effect of temperature and thermodynamics

A series of 125ml stoppered bottles containing 10 ml of anionic dyes' solution [100 mg/L for MO and 150 mg/L for RB] and 0.005 g of MMT@CTAB at different temperatures [25-45]°C and optimum pH [8] were shaken for 60 min for MO and 120 min for RB in an equilibrated shaker at constant speed 150 rpm. The residual [MO and RB] dye concentration was determined after adsorption and filtration.

Thermodynamic parameters [adsorption enthalpy [ΔH^o], adsorption free energy [ΔG^o], and adsorption entropy [ΔS^o] are expressed in Eq. [9] and Eq. [10] and were calculating as following; ΔS^o and ΔH^o were calculated from the Eq. [10] intercept that equals ΔS^o /R and slope that equals $-\Delta H^o$ /R of Ln Kc vs. 1/T. As, gas constant which expressed as [R] equals 8.314 J/mol K[41].

$$\Delta Go = -RT\ ln\ KC \quad [9]$$

$$lnK_C = \frac{\Delta S^\circ}{R} - \frac{\Delta H^\circ}{RT} \quad [10]$$

2.6. Application

The spiking of the [100mg/L for MO and 150mg/L for RB] into the real water samples [seawater and tap water] was carried out. Prior to the spiking of the dyes, the real water samples were digested by adding 0.5 g of $K_2S_2O_8$, and 5 ml H_2SO_4 98% [w/w] to 1000 ml of water sample and heated for 120 min at 90°C for complete digestion of presented organic materials. After cooling to room temperature, 0.005 g of MMT@CTAB modified clay was added to the prepared samples and the pH value was adjusted to 7 with continuous shaking for 60 min for MO and 120 min for RB. The solutions were centrifuged and again another 0.005 g of MMT@CTAB-modified clay was added to the supernatant to ensure the complete separation of analytes. The remaining MO or RB was determined using Unicam UV 2100 UV/Visible spectrometer at appropriate wavelengths.

3.Results and discussion

3.1. Optical images

Figure.1 [a-e] represents the MMT, MMT@CTAB, MMT@CTAB-MO, MMT@CTAB-RB and MMT@CTAB-MO/RB digital photographs, respectively. The difference in materials' color and shape is very noticeable as the material changed after reaction with CTAB from fine powder texture [Figure1a] to fine flakes [Figure1b]. This transformation is evidence of the modification occurrence. The change in the clay material' color before [MO, RB, and MO-RB mix] adsorption and after was counted as evidence of dye adsorption on the clay surface as the color changed from yellow [figure.2. a] of MMT@CTAB to bright orange in the case of MO adsorption, reddish pink in case of RB adsorption, and red in case of MO-RB mixture adsorption [Figure1 c-e]. Figure.2 [a-f] represents the [MO, RB, and MO-RB mix] before [Figure2 a, c, e] and after adsorption [Figure 2(b, d, f)] using the MMT@CTAB clay through batch experiments at the investigated ideal conditions.

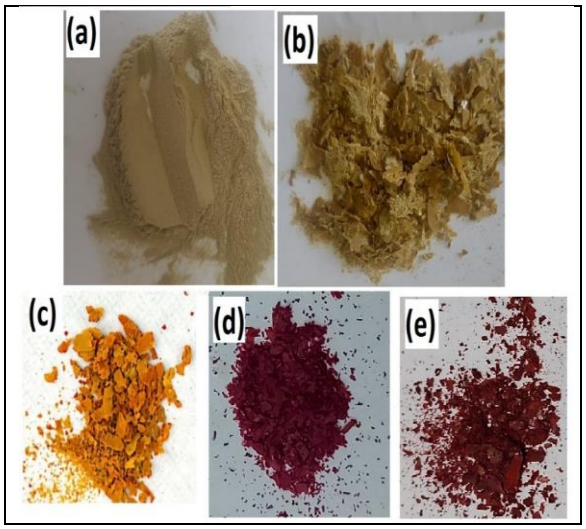

Figure1. Digital photographs of [a] MMT [b]MMT@CTAB [c] MMT@CTAB-MO [d] MMT@CTAB-RB [e] MMT@CTAB-MO/RB.

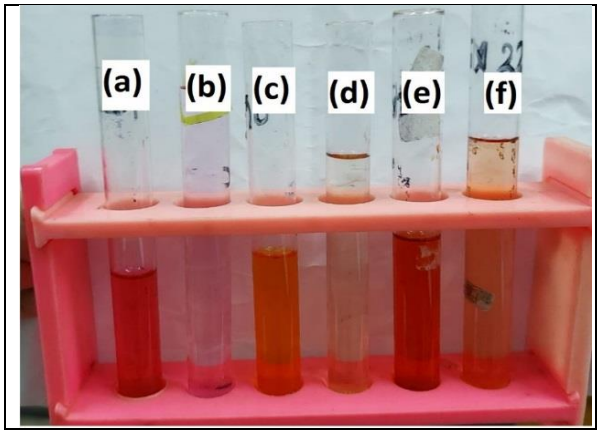

Figure 2. [a] RB anionic dye before adsorption, [b] RB anionic dye after adsorption, [c] MO anionic dye before adsorption, [d] MO anionic dye after adsorption, [e] MO-RB mixture before adsorption, and [f] MO-RB mixture after adsorption.

3.2. Characterization

3.2.1. FTIR analysis

MMT native clay and [MMT@CTAB] modified clay FTIR spectra were obtained and studied in the range of 400 cm^{-1} to 4000 cm^{-1}, which are present in [Figure3]. Both samples [MMT and MMT@CTAB] have some identical peaks, the first peak is Si-O which appeared in the two materials as follows; at approximately 466 cm^{-1} of the [Al-O-Al] vibrational band and 1029 cm^{-1} of the [Al-O-Si] vibrational band [42,43]. The other identical peaks are those that appeared at 1470 cm^{-1} and 690 cm^{-1} are related to Ca-Mg[CO_3]$_2$] and Al-O-Al vibrational bands, respectively [44]. There are three new bands appeared at 1647, 3442, and 3624 cm^{-1} corresponding to [–OH] deformation of water. The [CTAB] material Interaction with the MMT, native clay, was demonstrated by the appearance of CTAB characteristic peaks [–CH_3 vibrational band and –CH_2 vibrational band] [45,46].

FTIR spectra of MMT@CTAB before [MO and RB] adsorption is present in [Figure 4a] while after adsorption both materials; MMT@CTAB-MO and MMT@CTAB-RB spectra are shown in [Figure 4b] and [Figure 4c], respectively. It was noticed that the peak at 1395 cm^{-1} of MMT@CTAB FTIR spectra [Figure.4. a] was shifted to 1375 cm^{-1} with the peak intensity increasing in MMT@CTAB-MO [Figure 4 b] that may be attributed to SO_3^- stretching vibrational band [47]. MMT@CTAB-MO [Figure.4. b] and MMT@CTAB-RB [Figure 4c] have new peaks related to cyclic alkene [C=C] appeared at 1523 cm^{-1} for MMT@CTAB-MO and at 1520 cm^{-1} for MMT@CTAB-RB. Slight shifts occurred in the peak at 1647 cm^{-1} to 1612 cm^{-1} in MMT@CTAB-RB and to 1606 cm^{-1} in MMT@CTAB-MO. The peak at 4442 cm^{-1} became broader after MO and RB adsorption which may be attributed to hydrogen bond formation. There is another new peak appeared for MMT@CTAB-RB at about 1212 cm^{-1}, which is attributed to the [C-N] stretching band of RB. For MMT@CTAB-MO that present in [Figure 4b] and MMT@CTAB-RB [Figure 4c], new peaks that are associated with the C=C cyclic alkene appeared at 1523 cm^{-1} and 1606 cm^{-1}. Furthermore, the appearance of a new peak in MMT@CTAB-RB spectra attributed to C-N at 1212 cm^{-1} that may be attributed to the C-O stretching band of rose Bengal, as present in [Figure 4c]. Minor shifts related to the CH_3 and CH_2 stretching vibrational bands from 2852 cm^{-1} to 2846 cm^{-1} for [MMT@CTAB-MO] material and from 2852 cm^{-1} to 2847 cm^{-1} for [MMT@CTAB-RB] material [48–50].

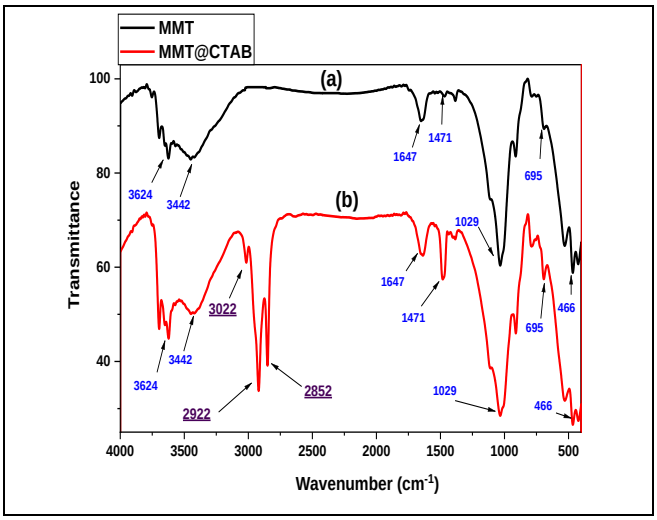

Figure 3. IR spectra of [a] MMT and [b] MMT@CTAB

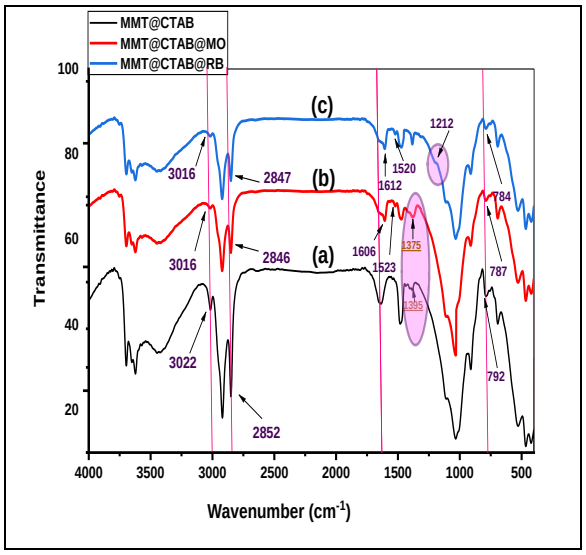

Figure.4. IR spectra of [a] MMT@CTAB, [b] MMT@CTAB-MO, and [c] MMT@CTAB-RB

3.2.2. Elemental analysis

The CHN analysis was evaluated for MMT and MMT@CTAB materials for proving the formation of the modified material [MMT@CTAB]. The results presented in Table 1 show the existence of nitrogen elements in the MMT@CTAB sample with a percentage [0.7 %] and the increase of carbon atom percentage from 1.567 % to 12.4 % and hydrogen atom percentage from 2.43 % to 3.98 %. These alterations are great evidence for the MMT clay modification of by CTAB.

Table 1: Elemental analysis of MMT and MMT@CTAB

Sample	C [%]	H [%]	N [%]
MMT	1.567	2.43	0
MMT@CTAB	12.4	3.98	0.7

3.2.3. SEM

The native montmorillonite clay [MMT] and modified clay [MMT@CTAB] surface morphology investigation was obtained utilizing the SEM technique. MMT and MMT@CTAB surface images are shown in Figure5a and Figure 5b, respectively. It was revealed that the MMT material modification results in more pores, flakes, and surface roughness in the modified montmorillonite clay [MMT@CTAB], and these alterations may be returned to the CTAB covering for the clay surface [38,51].

3.3. Adsorption studies

3.3.1. Point of zero charge [pH_{pzc}]

The pH_{pzc} of MMT@CTAB was obtained utilizing a previously published approach. For this purpose, 0.01 M NaCl solutions were applied and their pH was adjusted in the 2-12 range by using 0.1 M HCl or 0.1 M NaOH solution.

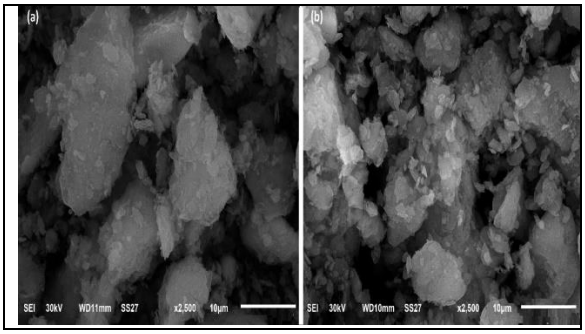

Figure5. [a] Native MMT and [b] MMT@CTAB SEM images.

Then, 0.1 g of the investigated material [MMT@CTAB] was added to these solutions and shaken for 48 h, and finally, the solution pH_{final} was calculated. Figure 6 shows the change of pH value [$pH_{initial}$-pH_{final}] of MMT@CTAB as a function of the $pH_{initial}$. From these findings, the pHpcz value of MMT@CTAB is determined to be 9.5. This shows that at pH below 9.5, the MMT@CTAB surface is considered to have a positive charge.

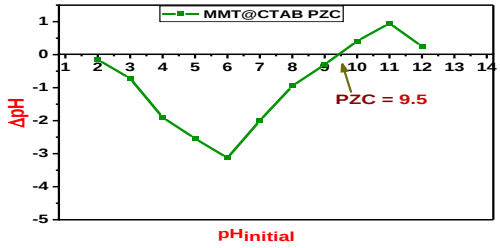

Figure 6 The pH_{pzc} of MMT@CTAB

3.3.2. Effect of pH

Solid-liquid interactions are highly affected by the aqueous solution' pH through the surface functional group protonation-deprotonation, so the pH parameter is very important to be studied [52,53]. So, the solution pH influence on the MO and RB anionic species removal using MMT@CTAB was investigated in the range of 2-11 for MO and 3-11 for RB. The investigation was obtained by using 10 ml of 100 mg/L of MO and 10 ml of 150 mg/L of RB and 0.005 grams of MMT@CTAB at room temperature. Figure 7 illustrates that the MMT@CTAB adsorption efficiency increased from 50% to 98.1% with pH increasing from 2 to 7 of the MO solutions and increased from 50% to 97.8% with pH increasing from 3 to 7 of the RB solutions. Then

at a pH above 7, both investigated dyes' adsorption efficiency decreased. From pH_{PZC} value [+ve < pH_{PZC} 9.5 < -ve], below pH_{PZC} the surface of MMT@CTAB is positive allowing the adsorption of anionic dyes. That is the main reason for increasing the adsorption of MO and RB adsorbed at pH [2-7] surface [the acidic media facilitates of the anionic dyes].

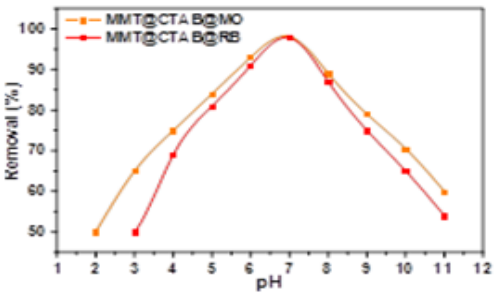

Figure.7. PH effect on MO and RB adsorption efficiency onto MMT@CTAB of these conditions [temp.: [30 °C], dose: 0.005 g., conc.: 100 &150 mg/L for MO and RB, respectively, volume: 10 mL].

3.3.3. Effect of dose

Adsorbent dose parameter investigation was obtained by using different amounts of MMT@CTAB in 10 ml 100 mg/L of MO / RB with a shaking time of 2 hours at room temperature. As shown in Figure 8, the capacity of MO adsorption increased from 170 mg/g to 196.2 mg/g with increasing MMT@CTAB dose from 0.0025 g to 0.005 g and the capacity of the RB adsorption increased from 160 mg/g to 195.6 mg/g with dose increasing from 0.0025 g to 0.005 g. With increasing the dose above [0.005 g], it was noticed that the capacity for MO adsorption decreased from 196.2 mg/g to 13 mg/g with a dose increasing from 0.005 g to 0.05 g and capacity of RB adsorption decreased from 195.6 mg/g to 10.662 mg/g with dose increasing from 0.005 g to 0.05 g. therefore, 0.005 g of MMT@CTAB adsorbent is considered a sufficient dose for MO / RB removal.

3.3.4. Initial concentration

The initial concentration parameter on MO/RB adsorption into MMT@CTAB surface was investigated in the range of [25-400] mg/L of the investigated anionic dyes [MO and RB] and the other conditions were kept constant. [Figure 9a] and [Figure 9b] represents the [MO and RB] initial concentrations' influence on the adsorption. It was noticed that the adsorption capacity for MO increased from 47.5 mg/g to 197.3 mg/g with [MO] initial concentration increasing from 25 to100 mg/L. Additionally, the adsorption capacity for RB enhanced from 49.8 mg/g to 297.346 mg/g with [RB] initial concentration increasing from 25 to 150 mg/L. At concentrations of more than 100 mg/L of MO and 150 mg/L of RB, the adsorption capacity remains constant. Therefore, it can be indicated that the MMT@CTAB adsorption reached equilibrium at a concentration of 100 mg/L and 150 mg/L for MO and RB, respectively.

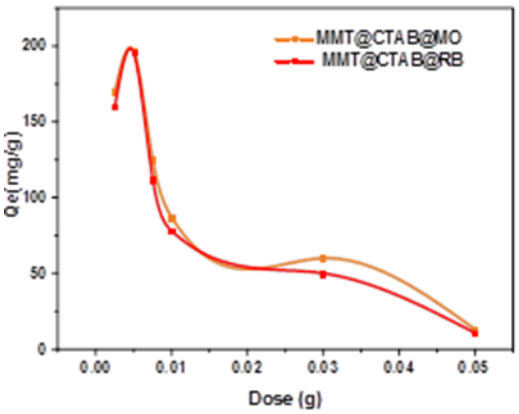

Figure8. Effect of dose on MO [100 mg/L] and RB [150 mg/L] adsorption onto MMT@CTAB at room temperature [30 °C] for 2hrs.

3.3.5 Isotherm studies

Langmuir and Freundlich's isothermal models were utilized in MO/RB adsorption into the MMT@CTAB adsorbent mechanism illustration. The two models' equations are present in Eq. [4] and Eq. [5] in the experimental section. Figure 10 represents Langmuir and Freundlich plots for MO and RB adsorption while Table2 shows the parameters [qm, KL, RL, n, KF] of the two investigated isothermal models. From these results, the Langmuir isothermal model is well-matched with MO and RB adsorption as its constants are more related to the MO/RB adsorption process with higher R2 values. R2 values for the Langmuir model are 0.99982 and 0.99982 for MO and RB removal, respectively while R2 values for the Freundlich model are 0.38949 and 5.7808*10-5 for MO and RB adsorption, respectively. So, the adsorption here was monolayer adsorption. Besides that, the estimated values of RL are calculated and they are founded to be less than 1 which proving that the suitability of MMT@CTAB to be utilized as an adsorbent material for the anionic species[19,27].

3.3.6. Oscillation time and Kinetics investigation

Contact time of [MO] and [RB] with MMT@CTAB adsorbent is a very essential parameter. So, it was investigated at different shaking times by using 0.005 g as a dose of MMT@CTAB adsorbent in pH-adjusted solutions [pH 7] of 100 mg/L of [MO] and 150 mg/L of [RB], and at room temperature. Figure.11 represents the influence of contact time on [MO] and [RB] anionic species adsorption [Figure11 a],

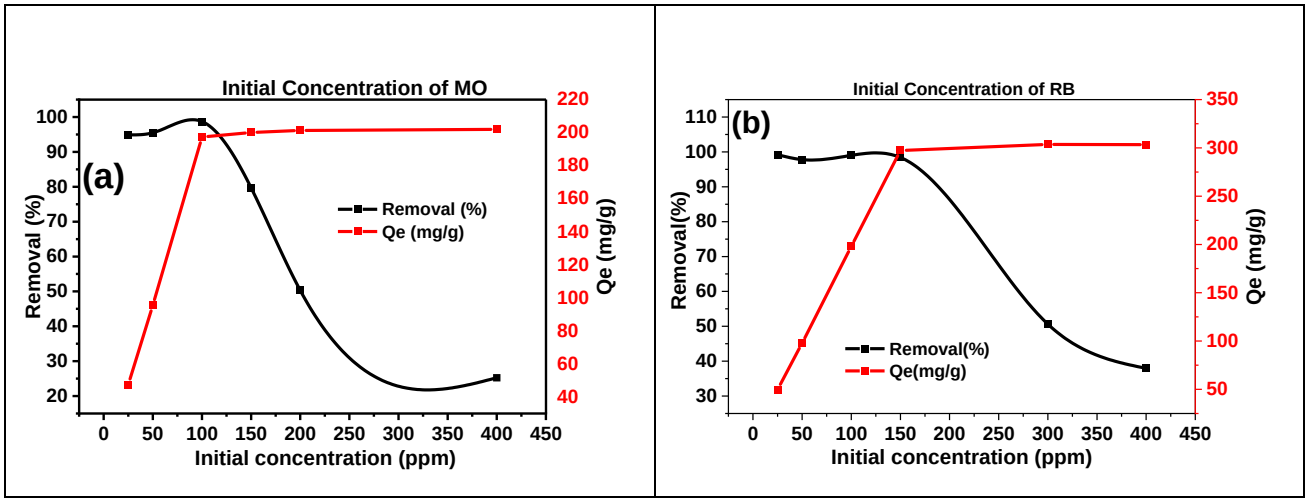

Figure 9. [a] Effect of initial concentration on MO adsorption, [b] Effect of initial concentration on RB adsorption

Table 2: Physicochemical adsorption of MO and RB by MMT@CTAB.

System	Langmuir isotherm constants			
	K_L[L/g]	q_m[mg/g]	R^2	R_L
MMT@CTAB-MO	0.5497	203.25	0.99982	0.01819
MMT@CTAB-RB	1.0897	304.878	0.99995	$6.11*10^{-3}$
System	**Freundlich isotherm constants**			
	K_F	N	R^2	
MMT@CTAB-MO	195.25	-5.000025	0.38949	
MMT@CTAB-RB	173.25	-1459.56	$5.7808*10^{-5}$	

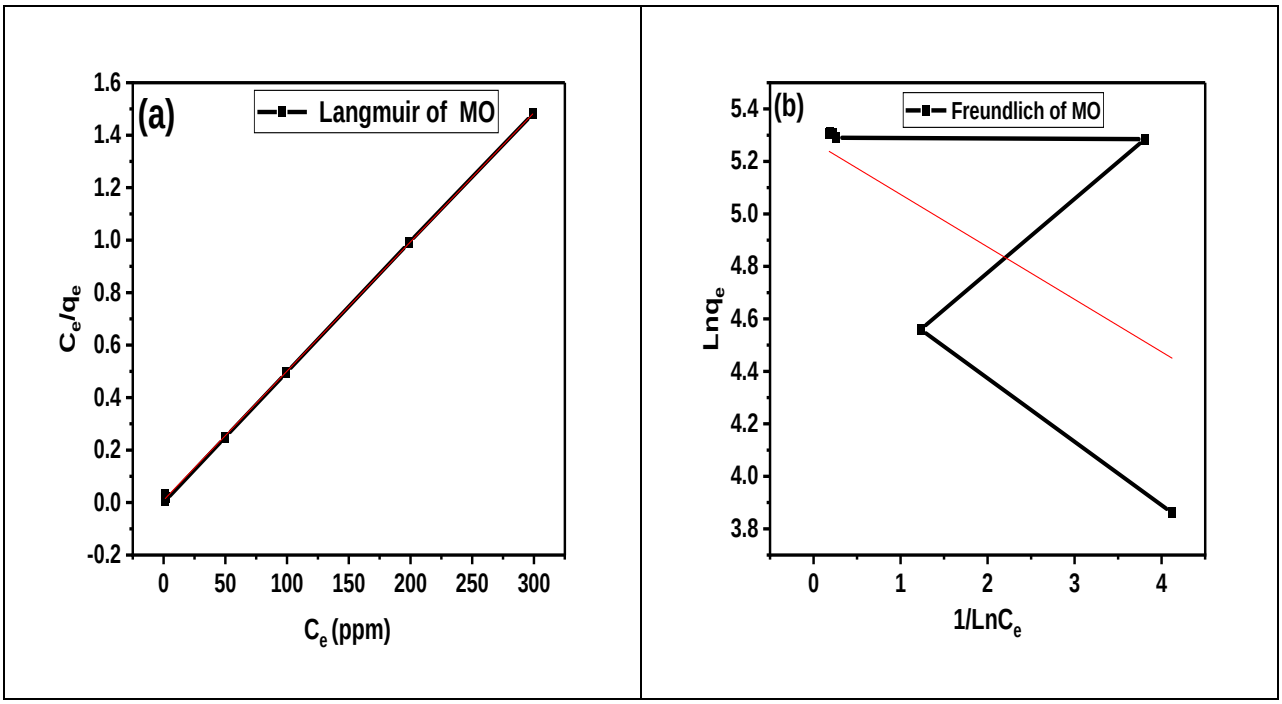

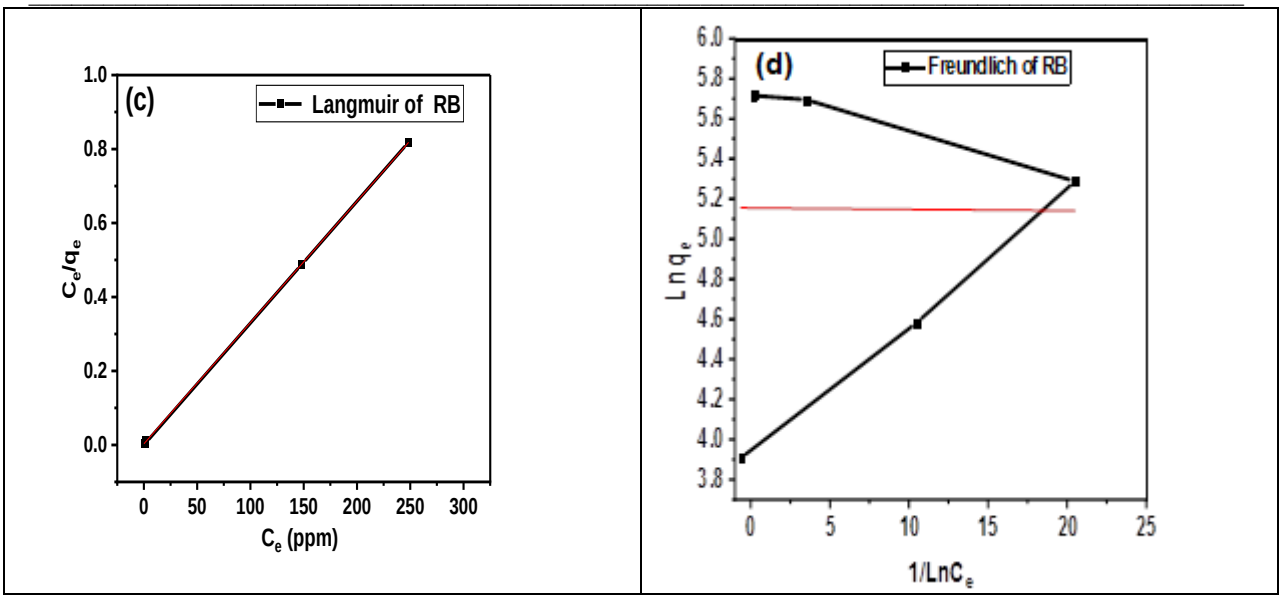

Figure.10. [a] Langmuir isotherm of MO adsorption, [b] Freundlich isotherm on of MO adsorption, [c] Langmuir isotherm of RB adsorption, and [d] Freundlich isotherm on of RB adsorption

pseudo-1st-order of anionic species [MO and RB] adsorption [Figure11b and Figure11d], and pseudo-2nd-order of Mo and RB adsorption [Figure 11c and Figure11e]. At began the adsorption is very fast as the efficiency at 15 min reached 84 % for MO and 75.33 % for RB. Then the MO removal efficiency increased from 84 % to 98.78 % with time increasing from 15 min to 60 min while the RB removal efficiency increased from 75.33 % to 98.8 % with shaking time increasing from 15 min to 120 min. With increasing shaking time of more than 60 min for MO and more than 120 min for RB, the efficiency stays constant which means that the removal efficiency reached equilibrium at 60 min for MO and 120 min for RB.

The two kinetic models; the pseudo-1st-order and the pseudo-2nd-order models [that are presented in Eq.7 and Eq.8, respectively] have been investigated for identifying the well-fitted model with MO / RB adsorption. Table 3 represents the estimated 1st and 2nd orders parameters [K_1, K_2, q_{e1}^{ads}, and q_{e2}^{ads}] and correlation coefficient R^2 values that obtained from each investigated model non-linear form. From these findings, MO/RB adsorption mechanism nature by the MMT@CTAB adsorbent can be illustrated. The calculated adsorption capacities in the case of pseudo-2nd-order for MO and RB were well-fitted with the experimental values. Besides that, R^2 values of pseudo-1st-order are very low 0.93764 for MO and 0.84677 for RB in comparison with those of pseudo-2nd-order 0.99988 for MO and 0.99891 for RB. Therefore, pseudo-1st-order cannot be used for explaining the adsorption nature here. So, MO/RB adsorption into MMT@CTAB adsorbent is well-fitted to pseudo-2nd-order and the adsorption rate-limiting step is controlled by a chemical process [38].

3.3.7. Effect of temperature and thermodynamics

The investigated free energy [ΔG^o], enthalpy [ΔH^o], and entropy [ΔS^o] thermodynamic parameters of the MO and RB anionic dyes adsorption by MMT@CTAB adsorbent were obtained by examining anionic dyes adsorption in a temperature range of 298-318 K. Thermodynamic parameters and Kc, equilibrium constant, were calculated as in [Eq.9] and [Eq.10]. Table 4 shows the estimated values of thermodynamic parameters While Figure12 shows the plotted curves. As can be seen, the estimated negative

Table 3: Kinetic parameters for the adsorption of MO and ARS by MMT@CTAB.

System	First-order model		
	K_1 [min^{-1}]	q_{e1ads}[mg/g]	R^2
MMT@CTAB-MO	3.176	202.07	0.93764
MMT@CTAB-RB	5.2797	297.6	0.84677
System	Second-order model		
	k_2 [g/[mg min]]	q_{e2ads} [mg/g]	R^2
MMT@CTAB-MO	$1.917*10^{-3}$	200.803	0.99988
MMT@CTAB-RB	$3.988*10^{-4}$	309.59	0.99891

Figure 11 [a] Effect of time on MO and RB adsorption on MMT@CTAB adsorbent, [b] Pseudo-1st-order for MO adsorption, [c] Pseudo-2nd-order for MO adsorption, [d] Pseudo-1st-order for RB adsorption, and [e] Pseudo-2nd-order for RB adsorption.

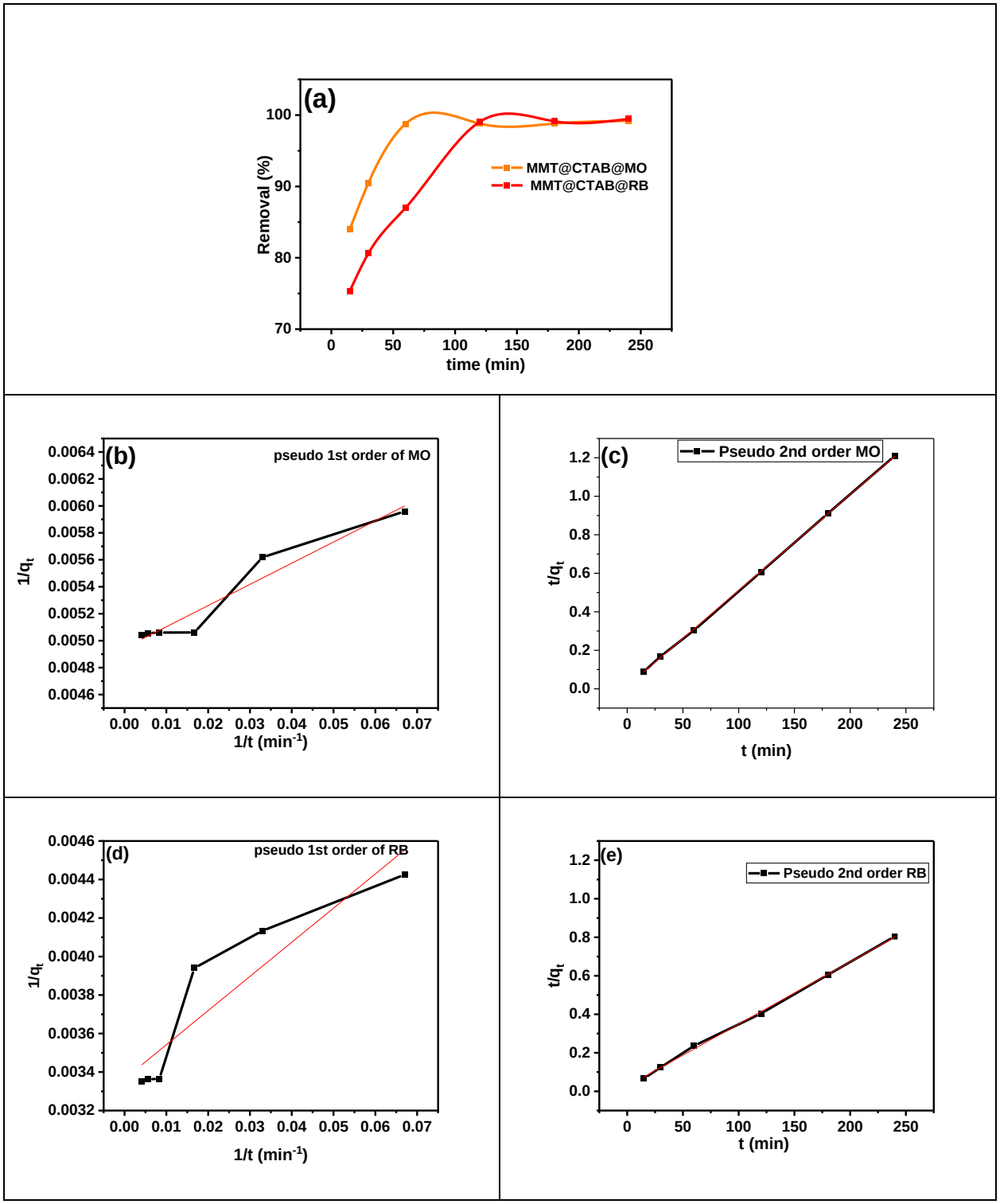

ΔG^o values prove that the MO and RB adsorption on MMT@CTAB adsorbent is spontaneous in addition to the thermodynamic feasibility of the MO and RB adsorption under the investigated temperature range. Also, negative charges of ΔH^o estimate that the adsorption process was exothermic for MO and RB adsorption. From ΔH^o values that are higher than

80Kj/mole, it was proven that the adsorption was chemisorption. Besides that, ΔS^o charge [negative] reveals that MO/RB adsorption results in a lower in randomness and an increase in alignment. It was noticed that the decreasing MO/RB adsorption with the temperature increase [19].

Table 4: Thermodynamic parameters for the adsorption of MO and RB onto MMT@CTAB

System	T [k]	K_c	ΔG^o_{ads} [KJ/mol]	ΔH^o_{ads} [KJ/mol]	ΔS^o_{ads} [J/mol K]
MMT@CTAB-MO	298	151.77	-12.651	-97.518	-280.167
	308	24.4	-9.759		
	318	13.87	-7.08		
MMT@CTAB-RB	298	244.073	-13.6	-92.513	-260.16696
	308	73.357	-10.999		
	318	23.119	-8.303		

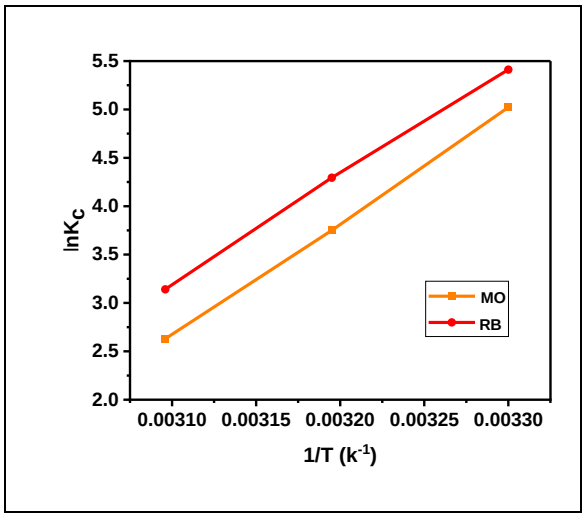

Figure 12. Plot of ln K_C as a function of reciprocal of absolute temperature [1/T] for the adsorption of [MO and RB].

3.3.8. Effect of ionic strength

As industrial wastewater has a high concentration of different solutes. So, the ionic strength parameter considers an important parameter. It was investigated using different anions such as NaCl [0.1M], Na_2CO_3 [0.1M], and EDTA [0.1M] at the optimum conditions of MO/RB adsorption. Figure 13 represents the influence of different anions on MO/RB adsorption on MMT@CTAB adsorbent. As shown in Figure13 for MO and RB adsorption on the MMT@CTAB surface, the different anions at concentration 0.1M don't significantly affect the MO/RB adsorption.

3.3.9. Desorption and Regeneration

In order to MMT@CTAB reusability investigation, 5 cycles of MO and RB adsorption-desorption were carried out at the optimum conditions. Several eluents were investigated and it was found that ethanol is the best among them. Figure 14a represents the effect of different eluents on the MO/RB desorption while Figure14b shows the obtained data of the repeated five cycles of MO and RB adsorption-desorption using ethanol as eluent.

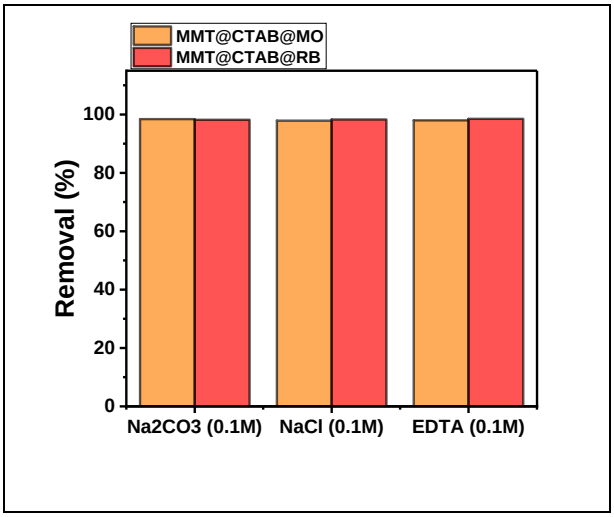

Figure.13. Effect of ionic strength on MO and RB adsorption.

3.3.10. Removal of MO and RB in Binary system

The maximum absorbance [λmax] of MO [466 nm], RB [549 nm], and [MO+RB] [547 nm] binary system are shown in Figure15a. It was observed that after mixing the two dyes [MO and RB] together, overlapping between the dyes was occurred and a new broader peak was formed at λmax equals 547 nm. All the adsorption investigations were examined at each pollutant λmax. As the organic pollutants [dyes] are present in real polluted water in multiple forms, so it is very essential to apply the MMT@CTAB clay material removal potential in the investigated dyes' binary systems. The binary system that contains 100 mg/L of MO and 150 mg/L of RB

was investigated by the batch procedures. Figure15b represents that the MMT@CTAB was more selective for RB than the MO as at the time of 15 min, the concentration of RB was decreased and the overlapping peak was changed to a lower value [527 nm]. [MO-RB]
mixture peak was shifted towards MO peak [480] at the time of 30 min. At a time more than that the peak wavelength became constant that may mean that the RB adsorption was completely adsorbed at time 30 min, and at this time the MMT@CTAB started to adsorb MO more quickly. The absorbance decreased from 1.595 to 0.12 with the contacting time passing from 30 min to 120 min.

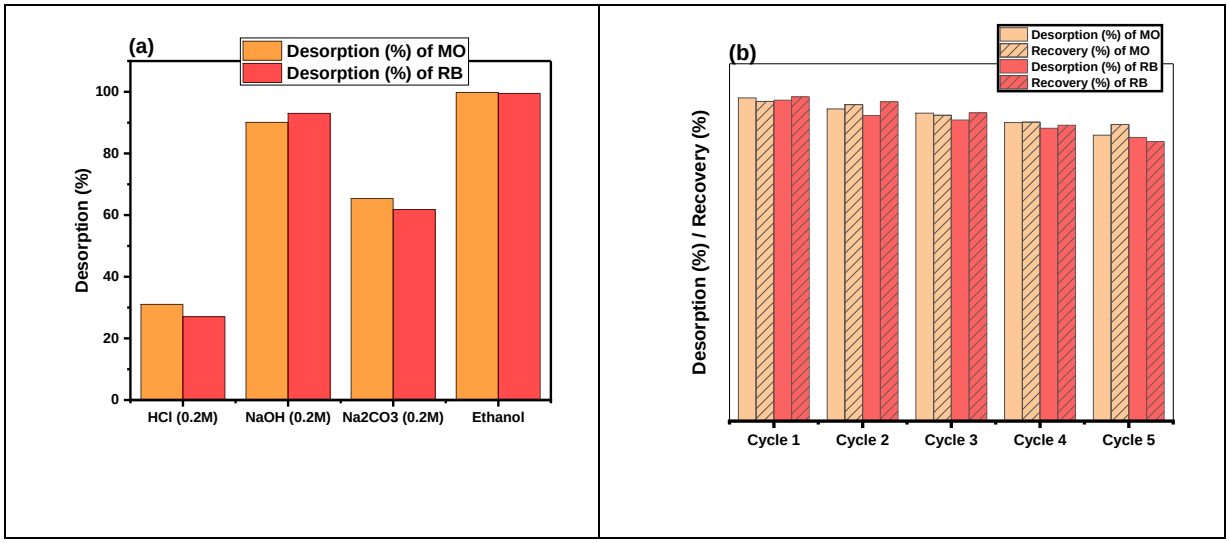

Figure14. [a] Desorption of MO and RB from MMT@CTAB adsorbent by different eluents [b] Repeated 5 cycles of MO and RB adsorption-desorption with using ethanol as an eluent.

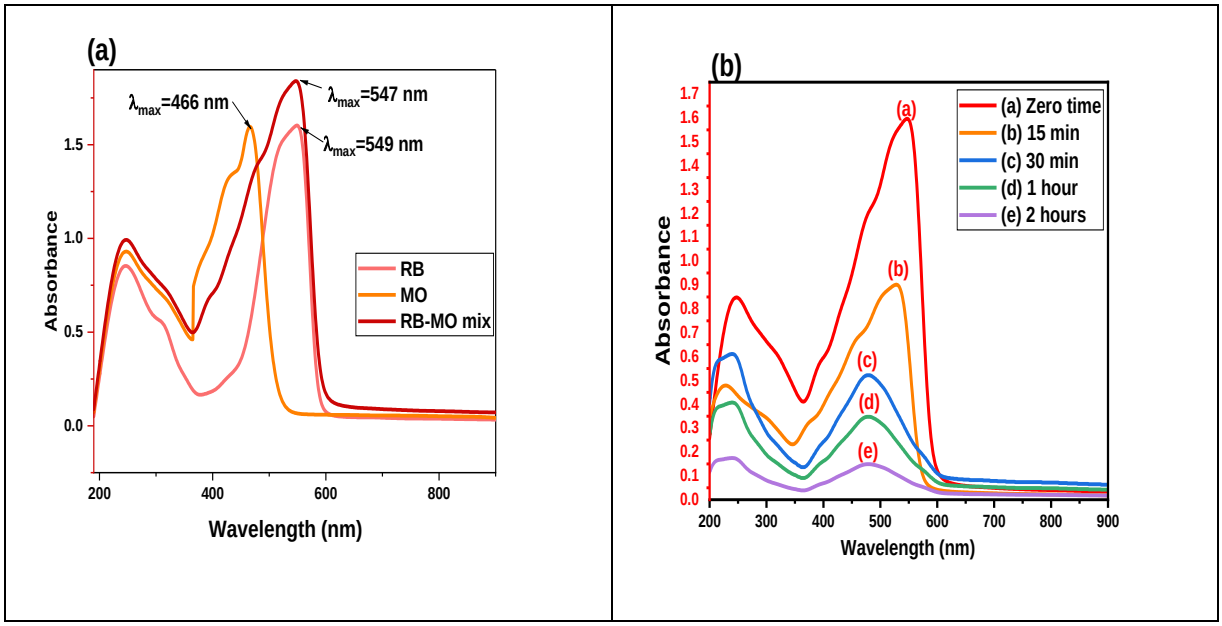

Figure 15: UV data of [a] MO, RB, and [MO-RB mix] [b] MO-RB mixture after adsorption by MMT@CTAB at different time intervals.

3.4. Optimization through column investigations

The removal of MO and RB anionic dyes by MMT@CTAB was investigated by applying column tests at optimum pH and temperature conditions [obtained from batch experiments]. The utilization of MMT@CTAB adsorbent as a filter was examined and the findings showed in Table 5, which showed that MO and RB dyes were removed with a percent

higher than 99% using 0.01 g of the MMT@CTAB adsorbent, a column with a diameter 0.7 cm at a slow flow rate for the two investigated dyes. The maximum capacity for RB was higher than that of MO.

Table 5: Column studies for the removal of the MO and RB anionic dyes

Dye	MMT@CTAB [gram]	Flow rate	Column diameter[cm]	Removal [%]	Adsorption capacity [mg/g]
Dose effect					
MO	0.002	fast	0.7	16.2	81
	0.005			43.9	87.8
	0.01			98.92	98.92
	0.0125			99.05	79.24
	0.015			99.5	66.33
	0.02			99.88	49.94
RB	0.002	fast	0.7	14.66	110
	0.005			44.5	133.6
	0.01			97.98	146.97
	0.0125			98.11	117.736
	0.015			98.59	98.59
	0.02			99.1	74.5
Diameter effect					
MO	0.01	fast	0.7	98.92	98.92
			0.9	90.8	90.8
RB	0.01	fast	0.7	97.98	146.97
			0.9	91.12	
Flow rate effect					
MO	0.01	fast	0.7	98.2	98.92
		slow		99.89	99.89
RB	0.01	fast	0.7	97.98	146.97
		slow		99.12	148.68

3.5. Application

3.5.1. In real water samples

The optimized experimental conditions were applied to real samples to evaluate the efficiency of MMT@CTAB for the adsorption of anionic dyes. By utilizing standard solutions, the calibration curves were obtained. The standard solutions [1.0 L] were prepared under the experimental conditions optimized above. The real investigated samples were tap water in our laboratory at Mansoura University and seawater in Damietta City. The obtained results are presented in Table 6. All spiked dyes were not naturally present in all of the samples. The recoveries were determined in the samples in which given amounts of each dye were spiked. The recoveries obtained were in the range of 97.93–99.42%. These findings indicate that MMT@CTAB adsorbent could be successfully applied to the determination of anionic dyes in real water.

Table 6: Analytical results of adsorption of MO and RB anionic dyes in real water samples utilizing MMT@CTAB adsorbent [n=5]

Sample	Dye	Spiked [µg mL^{-1}]	Measured [µg mL^{-1}]	Recovered [µg mL^{-1}]	Recovery [%]
Tap water	Methyl orange	0.00	0.00	0.00	0.00
		50	0.49	49.51	99.02
		100	1.9	98.1	98.1
	Rose Bengal	100	0.00	0.00	0.00
		100	0.9	99.1	99.1
		150	2.2	146.79	99.15
Sea water	Methyl orange	0.00	0.00	0.00	0.00
		50	0.446	49.554	99.108
		100	1.88	98.12	98.12
	Rose Bengal	0.00	0.00	0.00	0.00
		100	0.58	99.42	99.42
		150	3.105	146.895	97.93

3.6. Plausible mechanism of adsorption of MO and RB onto MMT@CTAB

The plausible **mechanism of adsorption of anionic species onto MMT@CTAB** can be discussed according to the findings of optical images of MMT@CTAB and the MMT@CTAB loaded dyes and the FTIR studies as it is represented in the following section. Adsorbate-adsorbent interaction mechanism through the adsorption process generally occurred through electrostatic interactions, ion exchanging, hydrogen bonds, etc [54,55].

Figure.16. [A] IR spectra of [A1] MMT@CTAB, [A2] MMT@CTAB-MO, and [A3] MMT@CTAB RB ;[B] schematic illustration of RB anionic species' adsorption on the MMT@CTAB adsorbent surface

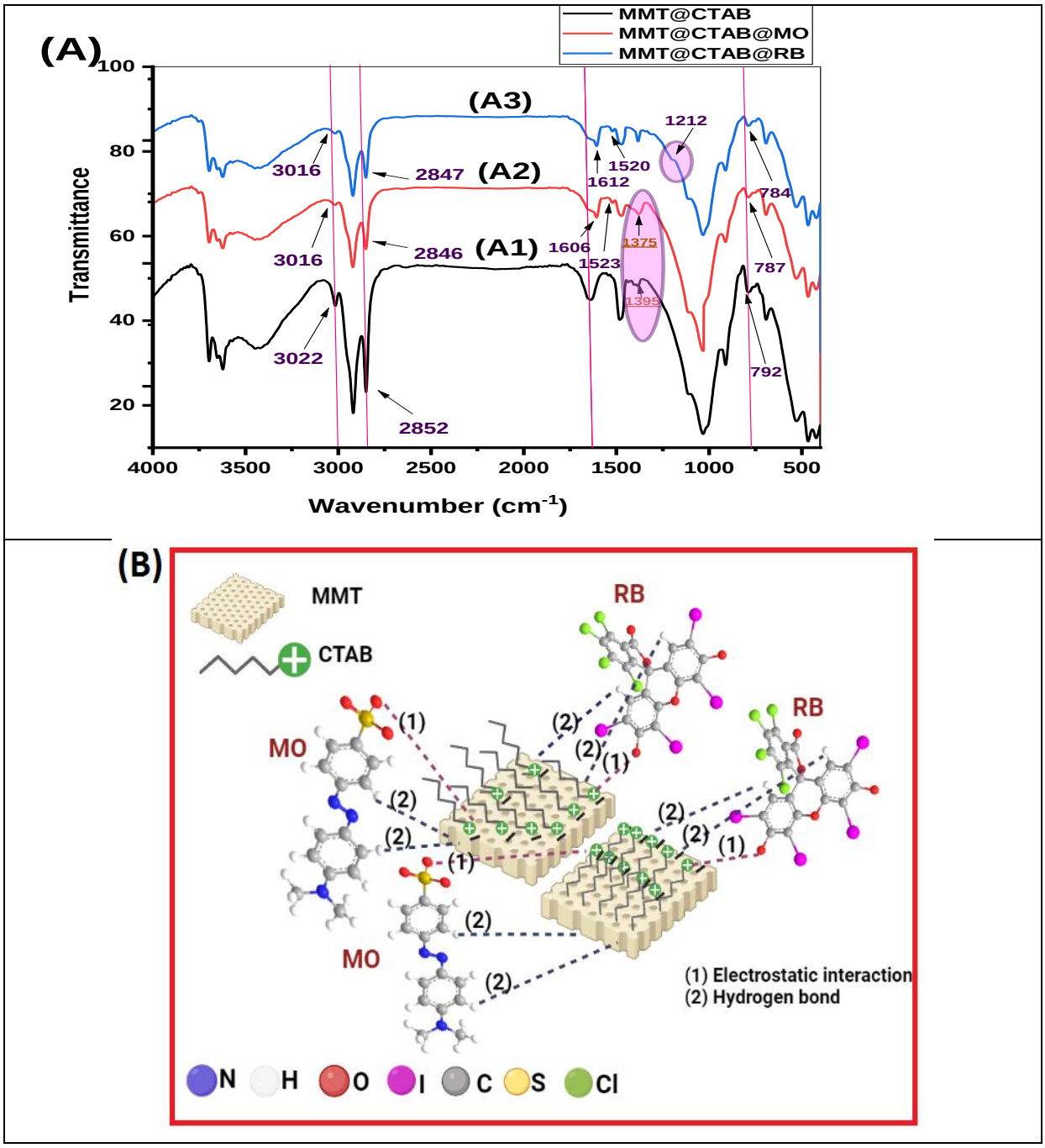

FTIR spectra after [MO] and [RB] anionic species adsorption on the [MMT@CTAB] adsorbent surface are highly efficient in the adsorption mechanism illustration. Significant changes were shown when the FTIR spectra of MMT@CTAB before MO and RB adsorption [Figure 16A1] compared to those after adsorption [[Figure16A2] and [Figure16A3]. The newly appeared peak at 1375 in MMT@CTAB-MO spectra is related to the sulfonate stretching

vibrational peak of MO dye [56]. Also, in [Figure16 A3], a new peak appeared at about 1212 cm^{-1} corresponding to the [RB] dye C-N stretching peak.
In both [Figure16A2] and [Figure16A3], New peaks that correspond to aromatic alkene C=C appeared at 1523 cm^{-1} for [MMT@CTAB-MO] and at approximately 1520 cm^{-1} for [MMT@CTAB-RB] [56, 57]. Slight shifts occurred in the peak at 1647 cm^{-1} to 1612 cm^{-1} in MMT@CTAB-RB and to 1606 cm^{-1} in MMT@CTAB-MO. The peak at 4442 cm^{-1} became broader after MO and RB adsorption which may be attributed to hydrogen bond formation. These new peaks are great evidence for MO and RB adsorption on the MMT@CTAB surface. CTAB characteristic bands still present with slight shifts after adsorption which confirm that CTAB doesn't leach into the solution during adsorption batch experiments. The aim of the modification here is to change the clay surface charge from -ve to +ve and to increase surface hydrophobicity. So, there are two expected interactions between investigated dyes [[MO] and [RB]] and MMT@CTAB material are;

Adsorbate	Adsorbent	Adsorbent dose	Initial concentration	Equilibrium time	Sorption capacity [mg/g]	Ref
MO	Co3o4 – nanoparticles [NPS]	0.5 g	50 mg/L	60 min	46.08	[58]
	magnetic lignin-based carbon nanoparticles [MLBCN]	20 mg/20 ml	120 mg/L	160 min	113.0	[59]
	biochar adsorbent [CMC]	1 g/l	75 mg/L	120 min	39.47	[60]
	Graphene oxide	20 mg	0.2 mg/L	100 min	63.69	[61]
	MMT@CTAB	0.0.005g/ 10ml	100 mg/L	60 min	203.25	Present study
RB	[MIP] chitosan-Tio2 nanocomposite[CTNC]	0.02g/50ml	3*10-5 mol/l	60 min	79.365	[62]
	1-naphthylammonium tetrachloroferrate	20mg	40 mg/L	30 min	20.70	[63]
	Pineapple leaves[PAL]	0.05mg/50ml	10 mg/L	180 min	58.8	[64]
	Mangifera indica homogenous powder	0.2g	20 mg/L	60 min	4.12	[65]
	MMT@CTAB	0.005g/10ml	150	120min	304.878	Present study

Table 7: Comparison of adsorption capacity of MO and RB onto MMT@CTAB with previously reported studies

1. Electrostatic interaction between the negative charge [that related to the O- a group of RB and SO_3^- of MO] and the positive charge of CTAB [$-N^+(CH_3)_3$] head.

2. The hydrogen bonding between OH group of MMT@CTAB material and the hydrogen group of [C_6H_6] ring in both MO and RB.

In Fig.16B, schematic illustration of adsorption mechanism of MO and RB anionic species' adsorption on the MMT@CTAB adsorbent surface is presented.

3.7. Performance of MMT@CTAB

The MMT@CTAB material provides the capability for MO and RB anionic species separation and removal from several water samples achieved with highly efficiency. Table [7] represents a comparison between the MMT@CTAB performances with other cited adsorbents. It was observed that MMT@CTAB material when comparing different adsorbents for remediation of MO and RB, the sorption capacity and the type of adsorbent, Adsorbent dose, Initial concentration and Equilibrium time on which the sorption is

performed should be taken into consideration. Finally, the MMT@CTAB has high capacities and efficiencies for the MO and RB recovery compared to other mentioned adsorbents as found in Table [7].

Conclusion:

In this paper, we modified the native MMT with CTAB and investigated its structure, characterization, and sorption behavior as a solution to water pollution issues found by the rise of the industrialization. Once the modified MMT material's cation exchange capacity [CEC] reached 1.0 CEC of pure MMT substance, the findings showed effective dye removal from the aqueous medium. A representative sorption analysis between MMT and MMT@CTAB showed that although the BET surface area significantly dropped after the modification process [m^2 g^{-1} to m^2 g^{-1}]. As a result, the MMT was much improved after being treated with the CTAB cationic surfactant, allowing it to more efficiently remove of the MO & RB anionic dyes. Maximum adsorption capacities of MO [203.25] and RB [304.878] mgg^{-1} were calculated using the Langmuir model. The kinetics of adsorption of both anionic dyes onto the MMT@CTAB were best described by the pseudo second-order model, and the isotherms were in accord with the Langmuir equation. The high values of correlation constant [R^2 = 0.99982& 0.99995] for MO & RB in the Langmuir isotherm suggested that sorption process had occurred on a homogenous and monolayer surface. Adsorption is an exothermic, spontaneous process, as shown by the derived thermodynamic function. It was observed that at low temperatures, the adsorption of MO and RB is a physical adsorption process based on hydrophobic interactions. The MMT@CTAB's pHpzc [9.5] is higher than the pH optimum [7] for anionic dyes. Reusability tests revealed that ethanol was the best regeneration eluent, and that MMT@CTAB could be used for at least four adsorption/desorption cycles. Based on the available information, we conclude that MMT@CTAB is a suitable adsorbent for the treatment of anionic dye wastewater owing to its simple production process, low cost, and successful application to a real-water samples.

References:

[1] WHO G. Guidelines for drinking-water quality. World Health Organization. 2017;55:1023–4.

[2] Karri RR, Ravindran G, Dehghani MH. Wastewater—sources, toxicity, and their consequences to human health. In: Soft computing techniques in solid waste and wastewater management. Elsevier; 2021. p. 3–33.

[3] Saleem J, Shahid U Bin, Hijab M, Mackey H, McKay G. Production and applications of activated carbons as adsorbents from olive stones. Biomass Convers Biorefin. 2019;9(4):775–802.

[4] Srivastav AL, Ranjan M. Inorganic water pollutants. Inorganic Pollutants in Water. 2020;1–15.

[5] Zamora-Ledezma C, Negrete-Bolagay D, Figueroa F, Zamora-Ledezma E, Ni M, Alexis F, et al. Heavy metal water pollution: A fresh look about hazards, novel and conventional remediation methods. Environ Technol Innov. 2021;22:101504.

[6] Muhammad N, Nafees M, Ge L, Khan MH, Bilal M, Chan WP, et al. Assessment of industrial wastewater for potentially toxic elements, human health (dermal) risks, and pollution sources: A case study of Gadoon Amazai industrial estate, Swabi, Pakistan. J Hazard Mater. 2021;419(March):126450.

[7] Berradi M, Hsissou R, Khudhair M, Assouag M, Cherkaoui O, El Bachiri A, et al. Textile finishing dyes and their impact on aquatic environs. Heliyon. 2019;5(11).

[8] Moore L. Textiles and clothing. Britain's Trade and Economic Structure. 1999.

[9] Affat SS. Classifications, advantages, disadvantages, toxicity effects of natural and synthetic dyes: A review. University of Thi-Qar Journal of Science. 2021;8(1):130–5.

[10] Farhan Hanafi M, Sapawe N. A review on the water problem associate with organic pollutants derived from phenol, methyl orange, and remazol brilliant blue dyes. Mater Today Proc. 2020;31(2020):A141–50.

[11] Hussain S, Kamran M, Khan SA, Shaheen K, Shah Z, Suo H, et al. Adsorption, kinetics and thermodynamics studies of methyl orange dye sequestration through chitosan composites films. Int J Biol Macromol. 2021;168:383–94.

[12] Akansha K, Chakraborty D, Ghosh S. Biocatalysis and Agricultural Biotechnology Decolorization and degradation of methyl orange by Bacillus stratosphericus. Biocatal Agric Biotechnol. 2019;18(December 2018):101044.

[13] Iwuozor KO, Ighalo JO, Emenike EC, Ogunfowora LA, Igwegbe CA. Adsorption of methyl orange: A review on adsorbent performance. Current Research in Green and Sustainable Chemistry. 2021;4:100179.

[14] Hassan AA, Sajid M, Tanimu A, Abdulazeez I, Alhooshani K. Removal of methylene blue

and rose bengal dyes from aqueous solutions using 1-naphthylammonium tetra chloroferrate (III). J Mol Liq. 2021;322:114966.
[15] Sharma S, Sharma A. Recent advances in photocatalytic manipulations of Rose Bengal in organic synthesis. Org Biomol Chem. 2019;17(18):4384–405.
[16] Khatri A, Rana PS. Visible light assisted photocatalysis of Methylene Blue and Rose Bengal dyes by iron doped NiO nanoparticles prepared via chemical co-precipitation. Physica B Condens Matter. 2020;579:411905.
[17] Ashraf RS, Abid Z, Shahid M, Rehman ZU, Muhammad G, Altaf M, et al. Methods for the Treatment of Wastewaters Containing Dyes and Pigments. 2021. 597–661 p.
[18] Waghchaure RH, Adole VA, Jagdale BS. Photocatalytic degradation of methylene blue, rhodamine B, methyl orange and Eriochrome black T dyes by modified ZnO nanocatalysts: A concise review. Inorg Chem Commun. 2022;109764.
[19] Akl MA, Hashem MA, Mostafa AG. Synthesis, characterization, antimicrobial and photocatalytic properties of nano-silver-doped flax fibers. Polymer Bulletin. 2022.
[20] Shi S hui, Liang Y, Jiao N. Electrochemical Oxidation Induced Selective C − C Bond Cleavage. 2020.
[21] Prusty S, Pradhan S, Mishra S. Ionic liquid as an emerging alternative for the separation and recovery of Nd, Sm and Eu using solvent extraction technique-A review. Sustain Chem Pharm. 2021;21(April):100434.
[22] Hube S, Eska M, Hrafnkelsdóttir KF, Bjarnadóttir B, Bjarnadóttir MÁ, Axelsdóttir S, et al. Science of the Total Environment Direct membrane fi ltration for wastewater treatment and resource recovery : A review. 2020;710.
[23] Rafaqat S, Ali N, Torres C, Rittmann B. Recent progress in treatment of dyes wastewater using microbial-electro-Fenton technology. RSC Adv. 2022;12(27):17104–37.
[24] Ouardi M El, Laabd M, Oualid HA, Brahmi Y, Abaamrane A. Efficient removal of p-nitrophenol from water using montmorillonite clay : insights into the adsorption mechanism , process optimization , and regeneration. 2019;19615–31.
[25] Yaghmaeiyan N, Mirzaei M, Delghavi R. Results in Chemistry Montmorillonite clay : Introduction and evaluation of its applications in different organic syntheses as catalyst : A review. Results Chem. 2022;4(July):100549.
[26] Zou W, Gao B, Sik Y, Dong L. Chemosphere Integrated adsorption and photocatalytic degradation of volatile organic compounds (VOCs) using carbon-based nanocomposites : A critical review. Chemosphere. 2019;218:845–59.
[27] Akl MA, Hashem MA, Ismail MA, Abdelgalil DA. Novel diaminoguanidine functionalized cellulose: synthesis, characterization, adsorption characteristics and application for ICP-AES determination of copper(II), mercury(II), lead(II) and cadmium(II) from aqueous solutions. BMC Chem. 2022 Dec 1;16(1).
[28] Wang LW, Wang RZ, Oliveira RG. A review on adsorption working pairs for refrigeration. Renewable and Sustainable Energy Reviews. 2009;13(3):518–34.
[29] Husien S, El-taweel RM, Salim AI, Fahim IS, Said LA, Radwan AG. Review of activated carbon adsorbent material for textile dyes removal: Preparation, and modelling. Current Research in Green and Sustainable Chemistry. 2022;100325.
[30] Shubbar AA, Sadique M, Kot P, Atherton W. Future of clay-based construction materials – A review. Constr Build Mater. 2019;210:172–87.
[31] Han H, Khalid M, Zhou T, Xu R. A critical review of clay-based composites with enhanced adsorption performance for metal and organic pollutants. 2019;369(February):780–96.
[32] Singla P, Mehta R, Upadhyay SN. Clay Modification by the Use of Organic Cations. Green and Sustainable Chemistry. 2012;02(01):21–5.
[33] Al Kausor M, Gupta S Sen, Bhattacharyya KG, Chakrabortty D. Montmorillonite and modified montmorillonite as adsorbents for removal of water soluble organic dyes: A review on current status of the art. Inorg Chem Commun. 2022;109686.
[34] Chen D, Chen J, Luan X, Ji H, Xia Z. Characterization of anion-cationic surfactants modified montmorillonite and its application for the removal of methyl orange. Chemical Engineering Journal. 2011;171(3):1150–8.
[35] Kiranşan M, Soltani RDC, Hassani A, Karaca S, Khataee A. Preparation of cetyltrimethylammonium bromide modified montmorillonite nanomaterial for adsorption of a textile dye. J Taiwan Inst Chem Eng. 2014;45(5):2565–77.
[36] Shirzad-Siboni M, Khataee A, Hassani A, Karaca S. Preparation, characterization and application of a CTAB-modified nanoclay for the adsorption of an herbicide from aqueous solutions: Kinetic and equilibrium studies. Comptes Rendus Chimie. 2015;18(2):204–14.
[37] Bayram T, Bucak S, Ozturk D. BR13 dye removal using sodium dodecyl sulfate modified montmorillonite: Equilibrium, thermodynamic, kinetic and reusability studies. Chemical

Engineering and Processing - Process Intensification. 2020;158(October):108186.
[38] Ouachtak H, el Guerdaoui A, Haounati R, Akhouairi S, el Haouti R, Hafid N, et al. Highly efficient and fast batch adsorption of orange G dye from polluted water using superb organo-montmorillonite: Experimental study and molecular dynamics investigation. J Mol Liq. 2021 Aug 1;335.
[39] Luo Z, Gao M, Yang S, Yang Q. Adsorption of phenols on reduced-charge montmorillonites modified by bispyridinium dibromides: Mechanism, kinetics and thermodynamics studies. Colloids Surf A Physicochem Eng Asp. 2015 Oct 5;482:222–30.
[40] Mostafa AG, El-Mekbaty A, Hashem MA, Akl MA. Selective separation of Cu(II) from a single metal Ion solution by using O-amino thiophenol-modified flax fiberd. Egypt J Chem. 2021 Apr 1;64(4):1701–8.
[41] Saleh MO, Hashem MA, Akl MA. Removal of Hg (II) metal ions from environmental water samples using chemically modified natural sawdust. Egypt J Chem. 2021 Feb 1;64(2):1027–34.
[42] el Haouti R, Ouachtak H, el Guerdaoui A, Amedlous A, Amaterz E, Haounati R, et al. Cationic dyes adsorption by Na-Montmorillonite Nano Clay: Experimental study combined with a theoretical investigation using DFT-based descriptors and molecular dynamics simulations. J Mol Liq. 2019 Sep 15;290.
[43] Huang Z, Li Y, Chen W, Shi J, Zhang N, Wang X, et al. Modified bentonite adsorption of organic pollutants of dye wastewater. Mater Chem Phys. 2017 Dec 1;202:266–76.
[44] Solotchina EP, Sklyarov E v, Solotchin PA, Vologina EG, Sklyarova OA. Mineralogy and crystal chemistry of carbonates from the Holocene sediments of Lake Kiran (western Transbaikalia): connection with paleoclimate. 2014; Available from: www.elsevier.com/locate/rgg
[45] Haounati R, Ouachtak H, el Haouti R, Akhouairi S, Largo F, Akbal F, et al. Elaboration and properties of a new SDS/CTAB@Montmorillonite organoclay composite as a superb adsorbent for the removal of malachite green from aqueous solutions. Sep Purif Technol. 2021 Jan 15;255.
[46] Vaia RA, Teukolsky RK, Giannelis' EP. Interlayer Structure and Molecular Environment of Alkylammonium Layered Silicates. Vol. 6, Chem. Mater. 1994.
[47] Bahrudin NN, Nawi MA, Jawad AH, Sabar S. Adsorption Characteristics and Mechanistic Study of Immobilized Chitosan-Montmorillonite Composite for Methyl Orange removal. J Polym Environ. 2020 Jul 1;28(7):1901–13.
[48] Avila MC, Lick ID, Comelli NA, Ruiz ML. Adsorption of an anionic dye from aqueous solution on a treated clay. Groundw Sustain Dev. 2021 Nov 1;15.
[49] Gamoudi S, Srasra E. Adsorption of organic dyes by HDPy+-modified clay: Effect of molecular structure on the adsorption. J Mol Struct. 2019 Oct 5;1193:522–31.
[50] Mallakpour S, Behranvand V. Polyurethane sponge modified by alginate and activated carbon with abilities of oil absorption, and selective cationic and anionic dyes clean-up. J Clean Prod. 2021 Aug 20;312.
[51] Shirzad-Siboni M, Khataee A, Hassani A, Karaca S. Preparation, characterization and application of a CTAB-modified nanoclay for the adsorption of an herbicide from aqueous solutions: Kinetic and equilibrium studies. Comptes Rendus Chimie. 2015 Feb 1;18(2):204–14.
[52] Ouachtak H, Akhouairi S, Ait Addi A, Ait Akbour R, Jada A, Douch J, et al. Mobility and retention of phenolic acids through a goethite-coated quartz sand column. Colloids Surf A Physicochem Eng Asp. 2018 Jun 5;546:9–19.
[53] Largo F, Haounati R, Akhouairi S, Ouachtak H, el Haouti R, el Guerdaoui A, et al. Adsorptive removal of both cationic and anionic dyes by using sepiolite clay mineral as adsorbent: Experimental and molecular dynamic simulation studies. J Mol Liq. 2020 Nov 15;318.
[54] Kamat P v. Photochemistry on Nonreactive and Reactive (Semiconductor) Surfaces. Vol. 93, Chem. Rev. 1993.
[55] Amosa MK, Jami MS, Alkhatib MFR. Electrostatic Biosorption of COD, Mn and H2S on EFB-Based Activated Carbon Produced through Steam Pyrolysis: An Analysis Based on Surface Chemistry, Equilibria and Kinetics. Waste Biomass Valorization. 2016 Feb 1;7(1):109–24.
[56] Liu A, Wang CC, Wang C zheng, Fu H fen, Peng W, Cao YL, et al. Selective adsorption activities toward organic dyes and antibacterial performance of silver-based coordination polymers. J Colloid Interface Sci. 2018 Feb 15;512:730–9.
[57] Ziane S, Bessaha F, Marouf-Khelifa K, Khelifa A. Single and binary adsorption of reactive black 5 and Congo red on modified dolomite: Performance and mechanism. J Mol Liq. 2018 Jan 1;249:1245–53.

[58] Uddin MK, Baig U. Synthesis of Co3O4 nanoparticles and their performance towards methyl orange dye removal: Characterisation, adsorption and response surface methodology. J Clean Prod. 2019 Feb 20;211:1141–53.
[59] Ma Y zhi, Zheng D feng, Mo Z ye, Dong R jing, Qiu X qing. Magnetic lignin-based carbon nanoparticles and the adsorption for removal of methyl orange. Colloids Surf A Physicochem Eng Asp. 2018 Dec 20;559:226–34.
[60] Yu J, Zhang X, Wang D, Li P. Adsorption of methyl orange dye onto biochar adsorbent prepared from chicken manure. Water Science and Technology. 2018 Mar 1;77(5):1303–12.
[61] Robati D, Mirza B, Rajabi M, Moradi O, Tyagi I, Agarwal S, et al. Removal of hazardous dyes-BR 12 and methyl orange using graphene oxide as an adsorbent from aqueous phase. Chemical Engineering Journal. 2016 Jan 15;284:687–97.
[62] Ahmed MA, Abdelbar NM, Mohamed AA. Molecular imprinted chitosan-TiO2 nanocomposite for the selective removal of Rose Bengal from wastewater. Int J Biol Macromol. 2018 Feb 1;107(PartA):1046–53.
[63] Hassan AA, Sajid M, Tanimu A, Abdulazeez I, Alhooshani K. Removal of methylene blue and rose bengal dyes from aqueous solutions using 1-naphthylammonium tetrachloroferrate (III). J Mol Liq. 2021 Jan 15;322.
[64] Hassan SS, El-Shafie AS, Zaher N, El-Azazy M. Application of Pineapple Leaves as Adsorbents for Removal of Rose Bengal from Wastewater: Process Optimization Operating Face-Centered Central Composite Design (FCCCD). Molecules. 2020 Aug 1;25(16).
[65] Sriram A, Swaminathan G. Removal of Rose Bengal dye from aqueous solutions using biosorbent obtained from Mangifera indica. Vol. 27, Indian Journal of Chemical Technology. 2020.